A Universal Retinal Image Template for Automated Screening of Diabetic Retinopathy

V. V. Starovoitov[a],*, Yu. I. Golub[a],, and M. M. Lukashevich[b],*****

[a] *United Institute of Informatics Problems, National Academy of Sciences of Belarus, Minsk, 220013 Belarus*
[b] *Belarusian State University of Informatics and Radioelectronics, Minsk, 220013 Belarus*
**e-mail: valerys@newman.bas-net.by*
***e-mail: 6423506@gmail.com*
****e-mail: lukashevich@bsuir.by*

Abstract—Diabetic retinopathy (DR) frequently appears in diabetic patients. It is initially asymptomatic, but can progress to blindness. Screening studies for its diagnosis are performed in many countries by means of photographing the eye retina with special fundus-cameras. These studies are aimed at revealing the presence of microaneurysms (MAs) on the retina, which are the primary signs of DR. The wide variety of cameras, peculiarities of retina illumination, FOV angles, and sizes of digital images has complicated the development of a reliable and universal approach to analyzing retina images by machine-learning methods. In this paper, we consider the problem of choosing the size and shape of a unified template for representing the data of an arbitrary retinal image for subsequent automated DR screening. It is experimentally proved that it is possible to extract a square inscribed in the FOV region from each retinal image and compress it to the size of 512 × 512 pixels. This is the minimum allowable size of the template. It preserves the required number of MAs for DR screening by machine-learning methods.

Keywords: digital retinal image, fundus-camera, microaneurysm, optical disk, machine learning
DOI: 10.1134/S1054661822020195

INTRODUCTION

Several diseases of the eye, especially in diabetic patients, are initially absolutely asymptomatic. Some of them, including diabetic retinopathy (DR), are refractory; therefore, it is of crucial importance to diagnose them at an early stage. Primary diagnostics is performed through screening of people by means of photographing the eye retina with special fundus-cameras [23]. A fluorescein angiogram (FAG) is the most efficient way to detect microaneurysms (MAs) on the retina, but it is not used for DR screening because of invasiveness and cost. The number of MAs on the retina is an important indicator of the development and progression of DR. It is assumed that MAs are not benign neoplasms. Treatment of DR at the early stages allows its course to be stabilized and decelerated; thus, analysis of the presence of microaneurysms on the eye retina may be of use in clinical practice [19].

The representation of the retinal region on an image depends on the spatial angle (field of view, or FOV) of the camera photographing it (see Fig. 1 and Table 1); therefore, it is frequently called the FOV region. The rest of the image is occupied by dark background. Cameras of different manufacturers register images on arrays of different sizes, differently placing the FOV region on the image (Fig. 2). The largest and smallest images in the Kaggle base (the largest available one [8]) have sizes from 5184 × 3456 to 433 × 289 pixels, respectively. The FOV angles in this base are different, but not specified. The resolution of the image and the ratio of the retinal image to the area of the array in pixels may vary in a wide range (Fig. 2). The area of the FOV region in the image ranges from 43.19% (in the Kaggle data-set [8]) to 99.09% in the DRIMDB base [2].

The thickness of the retina is different in different places. It depends on the age of the person and the presence of diseases [9] and on average it is approximately 250 ± 22 μm. The retina is riddled with blood vessels; therefore, red color dominates on the images registered in the visible range.

Table 1. FOV angles of different cameras and the corresponding retinal area on the image [11]

FOV angle, deg	Retinal area, mm^2
30	56.4
40	99.2
45	124.8
50	153.1

Received January 21, 2022; revised January 21, 2022; accepted January 21, 2022

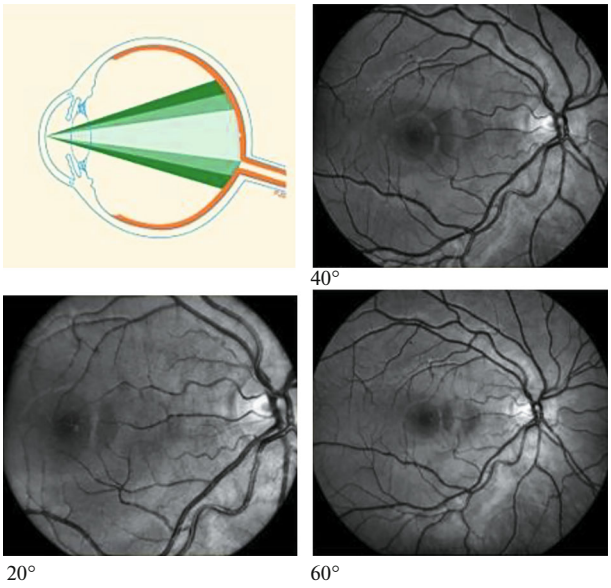

Fig. 1. Different projections of retina of the same eye obtained by cameras with different FOV angles (20°, 40°, and 60°); the light spot to the right is the OD [7].

Nunes et al. [14] described decadal studies of colored photos of patients' retina with macular edema. They showed that the rate of formation of microaneurysms is 9.2 ± 18.2 per year during the first two years. The authors concluded that the high rate of formation of microaneurysms of the fundus is a good biomarker of DR progression in patients with type 2 diabetes.

A detailed analysis of images of different eyes made by the same camera under the same conditions of photography showed that the size of the FOV mask in the image matrix and its boundaries and center can vary somewhat for images of different eyes. This is confirmed by the FOV masks constructed for high-resolution retinal images in the DRIVE database [3]. In this base, for each image a reference mask of the FOV region is presented, which has the same size as the image itself (52 336 × 3504 pixels). In Table 2 we present the areas, the coordinates of the centers of the FOV areas, and the correlation coefficients of the masks of three images from this database.

Small differences in the masks made by the same camera may be explained by the anatomical features of different persons and head position at the time of photographing, because the retinal image is a projection onto the spheroidal surface of the eyeball. These facts indicate that the FOV mask must be constructed for each image individually even if they are made by a single camera. Some retinal images contain the entire disk of the FOV region, while the disk is cropped from above and below in some images (Figs. 2 and 3).

1. PROBLEM FORMULATION

When methods of artificial intelligence are used for analyzing retinal images, these images must be reduced, preferably until a certain fixed size and shape of representation of the FOV region.

Here there arises a problem not formulated previously: to determine the universal shape and size of the matrix-template for representing an arbitrary retinal image with preservation of details sufficient for correct determination of the presence of diabetic retinopathy (DR) by machine-learning methods.

Concerning the shape, three variants are possible: (a) the disk of the FOV region, (b) a rectangle circumscribed around the FOV region, and (c) a square inscribed in it. To reduce the effect of edge distortions, the disk radius is sometimes decreased by 10%.

Concerning the size, the area of the image separated for analysis is usually transformed (reduced) to a square. Different square sizes are used. Most methods of artificial intelligence apply artificial neural networks trained for analysis of images of a fixed size, most frequently 512 × 512 or 256 × 256 pixels. Therefore, the original retinal images are scaled to a matrix of the size for which the applied network is trained, independently of the above-indicated peculiarities [9]. In review [4] it was stated that researchers scale the original retinal images into square ones with sizes of 180 × 180, 224 × 224, 227 × 227, 231 × 231, 416 × 416, and 512 × 512 pixels, and even up to 1200 × 1800 pixels. However, it is clear in Fig. 1 that the proportions of

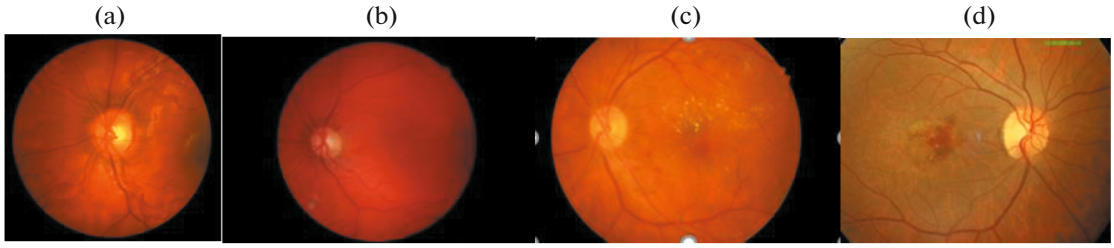

Fig. 2. Examples of retinal images from different databases: (a) CHASEDDB1, FOV = 30°, 999 × 960 pixels in size; (b) DIARETDB1, FOV = 50°, 3504 × 2316 pixels; (c) IDRID, FOV = 50°, 4288 × 2848 pixels; and (d) DRIMDB, FOV = 60°, 760 × 570 pixels.

Table 2. Examples of parameters of FOV mask on images with size 52336 × 3504 made by one camera

File name	Coordinates of center (x, y)	Area of mask, pixels	Correlation coefficient of masks
A1 = 01_dr_mask	1759.6, 1166.8	6912991	(A1, A2) = 0.9985
A2 = 02_dr_mask	1758.9, 1166.9	6915024	(A1, A3) = 0.9987
A3 = 03_dr_mask	1759.8, 1166.8	6915830	(A2, A3) = 0.9982

anatomical objects and disease attributes will be represented by different numbers of pixels on the images unified in this way. It is clear that the original images must be reduced.

There arises a question: how should we reduce the retinal image to be able to recognize individual microaneurysms in it? This is because the main attribute of the DR is the appearance of microaneurysms on the retina [22]; their description as micro clearly indicates the smallness of their size. Microaneurysms are isolated spots of circular shape and of varying sizes. They appear from the inner layers of the retina as a result of generation of new blood vessels or as a result of hemorrhage through the weakened walls of capillary vessels [23]. They are dark-colored (on colored images they are dark red) and are characterized by local minimums of brightness values. Blood vessels may have similar brightness values, but they have no pronounced local minimums and are elongated objects.

When analyzing retinal images, it is important to take into account the size of MAs in pixels and their correspondence to the dimensions in microns. In the literature sources we find various estimates for the physical dimensions of MAs. Nunes et al. [14] said that they may have dimensions from 10 to 125 μm. According to the studies of Wang et al. [21], the diameter of microaneurysms is 104 μm on average (ranging from 43 to 266 μm). In other works the following dimensions of microaneurysms are given:

– from 10 to 100 μm [20];
– from 14 to 136 μm [12];
– from 10 to 100 μm [15];
– from 10 to 125 μm [17];
– from 15 to 60 μm [6, 18, 24].

Elloumi et al. [5] obtained high-resolution confocal images of the eye retina of a person with diabetes and quantitatively estimated the distribution of the sizes of MAs. The average diameter of MAs was 34 ± 16 μm, and 60% of them were less than 40 μm in diameter. Elloumi et al. determined the critical diameter of a MA to be 15 μm for those generated by capillary vessels, 25 μm for those generated by venules, and 104 μm for those generated by arterioles (Table 3). They stated that it is easy to identify large MAs, which pose no danger, but that smaller MAs with diameters less than 20–30 μm are not identified by standard angiography because they appear as background leakage of blood through the retina. Although modern methods of visualization cannot detect small MAs, modern methods of ophthalmological diagnostics, such as OCT, reach a resolution of 2 μm, and small MAs are clearly seen. The cost of such diagnostics, however, is considerably higher, making it not feasible for screening studies.

In contrast to microaneurysms, the optical disk (OD) of the retina has similar dimensions from person to person. Ophthalmologists have established that the

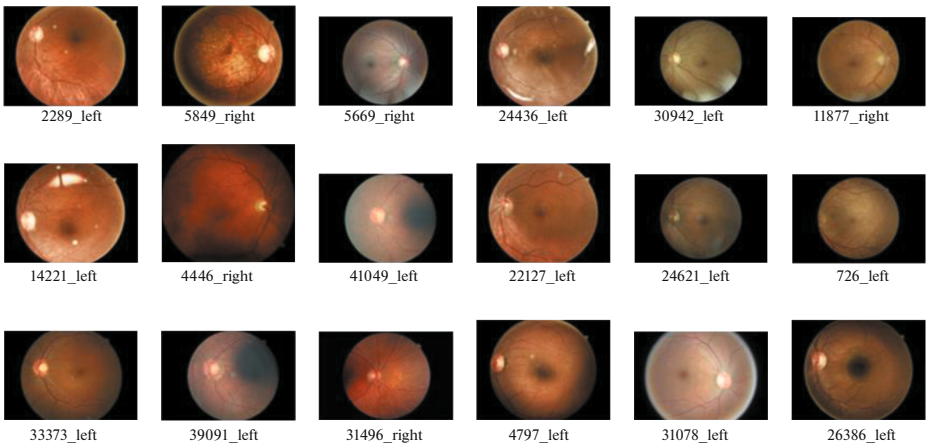

Fig. 3. Variety of retina representation in the images of Kaggle-2015 database.

Table 3. Ratio of critical sizes of microaneurysms and blood vessels

Blood vessels	Diameter, μm	Width of MA, μm
Capillaries	10	15
Venules	20	25
Arterioles	50	104

OD of a healthy human eye has an oval shape with average dimensions of 1.88 mm in the vertical direction and 1.77 mm in the horizontal direction [19, 24]. The dimensions may slightly differ between men and women and persons of different races, but the standard deviation is not larger than 0.19 mm. The OD is registered differently by cameras of different manufacturers; i.e., the resolution of photo images, as well as the representation of the OD in pixels and the region of the retina appearing in the frame, vary (Fig. 1) [8], but the physical dimensions of the OD are approximately the same independent of the digital representation.

These facts allow estimating the range of values of microaneurysms in pixels independently of the FOV angle and camera resolution. The MA sizes mainly fall in the range from 1/15 to 1/150 of the vertical size of the OD for a normal eye both in microns and in pixels, i.e., roughly from 12.5 to 125 μm. However, their sizes in pixels are different in digital images made by different fundus-cameras. Let us check this statement experimentally.

2. EXPERIMENTAL DATA

At present, there are only three publicly available databases of images containing color retinal images and MA masks: E-ophtha (part of Kaggle-2015 base), the Chinese base DDR, and the Indian base IDRID. The IDRID base additionally contain the OD masks. All masks in these bases were formulated by qualified expert health professionals.

In the IDRID database there are 81 images with MAa. The angle FOV = 40°. All the images have the same size of 4288 × 2848 pixels, and the FOV region was somewhat cropped from above and below [16].

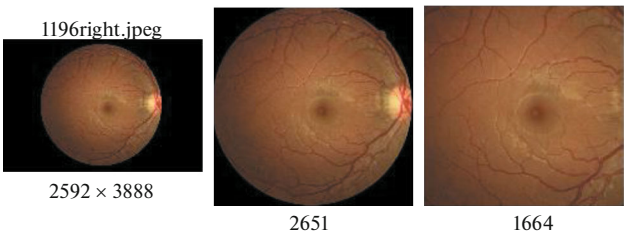

Fig. 4. (a) original image with 2592 × 3888 pixels (the ratio of the retina area to the image area is 0.4319); (b) circumscribing square K1 cropped from it and having side of 2351 pixels; and (c) square K2 with side of 1664 pixels.

In the DDR database there are 13673 images acquired at 147 Chinese hospitals [10]. The angle FOV = 45°. The base was created especially for studies associated with the DR screening. For 757 images, experts formed the masks for MA and other DR attributes. We used 487 images with MA masks. This base has a significant disbalance of classes; for instance, the share of images of eyes of normal persons is 45.84% of the entire database, and the share of images with moderately severe DR is 4.61%. In performing their studies, the authors of [10] cropped the rectangle circumscribing the FOV area and transformed it to a square with a size of 512 × 512 pixels.

In the E-ophtha database there are 148 images with MA masks and 233 images of normal eyes [1]. The angle FOV = 40°. There are four image sizes: 960 × 1440, 1000 × 1504, 1696 × 2544, and 1360 × 2048 pixels. A portion of the images have a cropped FOV area from above and below. Other images contain the full FOV area in the form of a circle. On average, there are 8.8 MAs with an average size of 47.2 pixels per image. The total area of all MAs in a single image is approximately 0.01% of the image area. Consequently, the MA areas may be reduced to those dimensions such that the information that allows their detection is preserved.

3. ANALYSIS OF DATA IN THE CHOSEN PART OF IMAGE OF FOV REGION

We describe the algorithm of cropping a square from a retinal image of arbitrary size. This consists of the following steps.

Step 1. Construct the binary mask of the FOV region in the image of the red color channel.

Step 2. From the mask, construct the rectangle P circumscribed in the FOV region.

Step 3. If P is a square (FOV is represented by a complete circle), K1 = P. Otherwise (i.e., when the FOV area is partially cropped), construct the square K1 inscribed in P with identically cropped segments of the FOV area in the horizontal and vertical directions.

Step 4. In the square K1, construct the square K2 < K1 inscribed in the FOV area. The K1 square contains the background segments, and the K2 square does not contain them.

Step 5. Reduce the K2 square to the specified size. In our experiments we reduced K2 to 512 × 512 pixels.

Examples of original images and cropped objects from them are presented in Figs. 4 and 5. The K2 square inscribed in the FOV region is 64% of the area of the complete circle of the FOV region. It is twofold less than the square circumscribing the FOV region. The side of the K1 square is $\sqrt{2} = 1.4142$ times larger than the side of the K2 square. The dimensions of the MAs differ in the same ratio if both squares are reduced to the same size in pixels.

A positive property of the inscribed square is the absence of background in the cropped background image, and the use of an individual mask for each image is not required in the further analysis.

On the example of images from the above-indicated bases, we estimate how the MA sizes vary after reducing the inscribed square to the size of 512 × 512 pixels. In Fig. 6 we provide the examples of placing the rectangles circumscribing the set of MAs and the squares inscribed in the FOV region for several images from the IDRID base. In Fig. 7 we provide the graphs of the number of MAs in all images of this base and inside the inscribed squares. In Figs. 8 and 9 we show the similar graphs for the images of the DDR database.

The analysis of the given graphs and images shows that a large part of the MAs fall into the square inscribed in the FOV region (sometimes, all MAs). Most frequently, MAs are located near the center. In Figs. 7b and 8b we see that the number of MAs not falling into the FOV square is not large. It increases as the total number of MAs in an image increases. If there are fewer MAs in the image, outside the square there are from 0 to 3 MAs. This means that the square inscribed in the FOV region contains a number of MAs sufficient for diagnosing DR during screening.

In Table 4 we provide the sizes of some studied images, the sizes of the rectangles P cropped from them, the sizes of the squares K1 and K2, and the ratios between the FOV area and the image area and between the indicated figures.

In the first row, we provide the data for images of the IDRID base and next for the images of the DDR base. In the column K2 : 512 we present the coefficients of compression of the K2 square to the size of 512 × 512 pixels. K1 : K2 means the ratio of the sizes of these squares. If it is less than 1.41, then the FOV region in the original image is partially cropped and K1 is constructed inside the rectangle P circumscribing the FOV region. In Table 4 P : 512 indicates the ratio of the larger side of the rectangle P to the side of the square of 512 × 512. Table 4 shows the alternatives for cropping the part of the retinal image to be used for subsequent DR classification.

We estimate to which size in pixels MAs are reduced in the case of cropping the squares in the images of the above-described bases.

Fig. 5. (a) Original image with 2336 × 3504 pixels (the ratio of the retina area to the image area is 0.6914); (b) circumscribing rectangle P cropped from it having the vertical size of 2224 pixels; and (c) square K2 with side of 2030 pixels.

Although all the images of the IDRID base are made by the same camera and have the same resolution, the dimensions of the OD were different. On average, the OD height was 105.15 ± 10.57 pixels in the K2 square with a size of 512 × 512 pixels. The graph of the heights is given in Fig. 10. The horizontal lines are the mean value and the mean-square error. These data tell us that the smallest MAs may be lost for subsequent analysis and we cannot analyze images less than 512 × 512 pixels in size cropped from the original retinal image.

The coefficient of compression of the inscribed square for the images of the IDRID base is 4.71. The lowest area of MAs in the original images is 17 pixels, and the size of this MA is approximately 4 × 4 pixels, i.e., approximately 130 times smaller than the OD. After compression of the image of the inscribed square K2 by 4.71 times to the size 512 × 512 pixels, the diameter of the smallest MA is less than 1 pixel. If we compress the rectangle P with a size of 2842 × 3412 pixels by 6.66 times, circumscribing the FOV region to dimensions of 512 × 512, then the width of the smallest MA reduces 6.66-fold and, taking into account rounding of the pixel coordinates to integers, becomes less than a single pixel. This means that the MA disappears in the image reduced to a size of 512 × 512 pixels. Even if the image of the MA is preserved after reduction, but has a size of 1–2 pixels, the classifier may think that this small spot is just a small pulse noise and ignore it as a feature.

In the DDR base, the compression coefficients are smaller, but, after cropping the K2 squares, the OD

Table 4. Image sizes and their aspect ratios

No.	Image size	FOV : S, %	P	K1	K2	K2 : 512	K1 : K2	P : 512
1	2848 × 4288	69.04	2842 × 3412	2848	2413	4.71	1.18	6.66
2	1536 × 2048	53.92	1468 × 1468	1468	1038	2.03	1.41	1.41
3	2100 × 2100	39.42	1487 × 1487	1487	1051	2.05	1.41	2.90
4	2976 × 2976	69.53	2798 × 2798	2798	1976	3.86	1.41	1.41
5	2000 × 2584	74.91	1958 × 1958	1958	1625	3.17	1.20	3.82
6	1904 × 2460	84.75	1865 × 2400	1865	1697	3.31	1.10	4.69

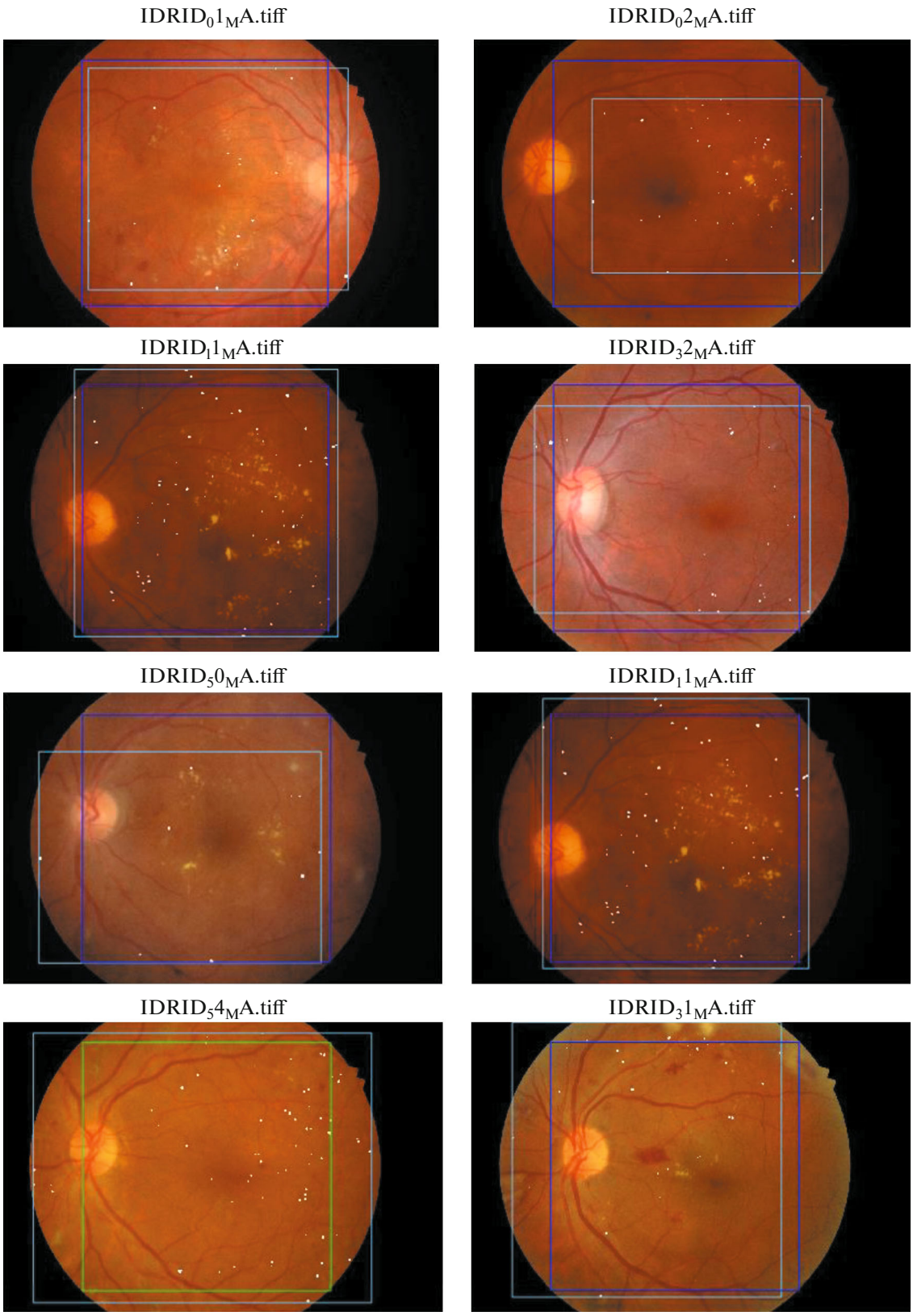

Fig. 6. In the images from the IDRID database, light rectangles describe the MA regions (white points); blue color shows the squares inscribed in the FOV region.

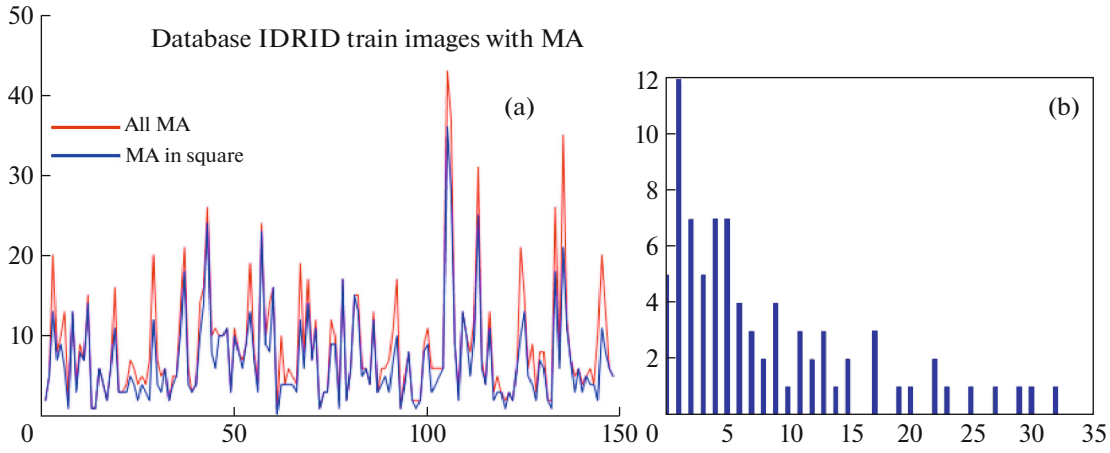

Fig. 7. (a) Distribution of MAs in images of the IDRID database: red curve is the number of all MAs in the image, and blue curve is the number of MAs falling into the inscribed square; (b) histogram of the difference of these values over all images of the IDRID database.

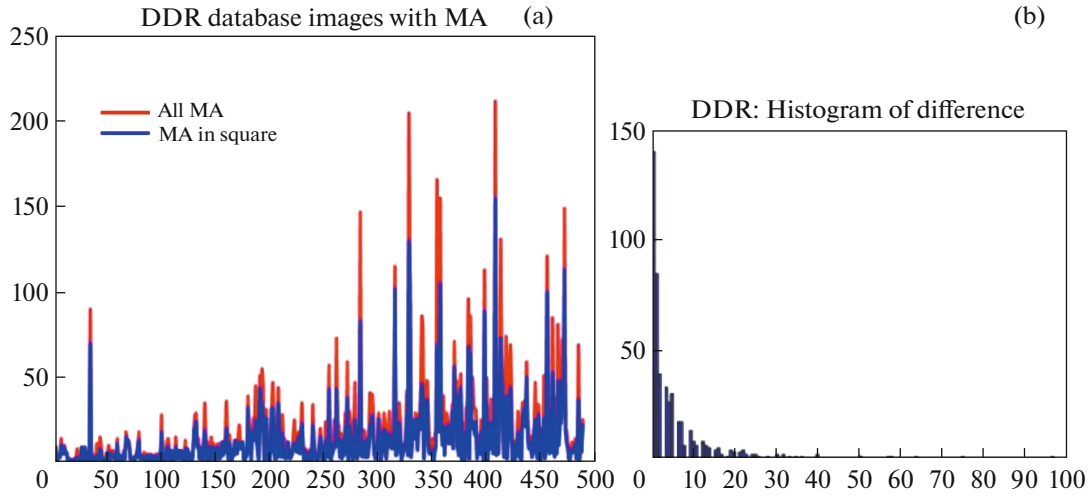

Fig. 8. (a) Distribution of MAs in images of the DDR database: red curve is the number of all MAs in the image, and blue curve is the number of MAs falling into the inscribed square; (b) histogram of the difference of these values over all images of the DDR database.

sizes are approximately the same. This indicates the invariancy of the OD representation on cropped retinal images independently of the resolution of the original images. There are no OD masks in this database, and we estimated the sizes on a sample basis using an interactive interface.

In Table 5 we provide the characteristics of four images from the IMRID base before and after reducing the image. 0*X* is the image number in the base and 0*X*square means the square inscribed in the FOV region reduced to the size of 512 × 512 pixels. Next is the number of MAs in the original and cropped images. The minimum and maximum sizes of MAs and ODs for original and reduced images are given. The sizes of the smallest MAs after scaling the square are 1–2 pixels in width or height.

The last column of Table 5 gives an approximate pixel size in microns following from the average OD height of 1880 μm. If we do not compress the square, not inscribed, but circumscribed about the FOV region, the MA sizes become smaller by 1.4142 times, i.e., many (up to rounding to integer numbers) of them disappear. It is clear that if we transform the FOV region to a smaller square, for instance, with a size of 224 × 224 pixels, as Noriega et al. [13] did for their screening system, then a significant share of small MAs are overlooked and the screening results become less reliable. After such transformation, the size of one pixel corresponds to approximately 34 μm.

The data given in Table 5 show that the image used for classification must not be smaller than 512 × 512 pixels. This is the minimum size permitting the

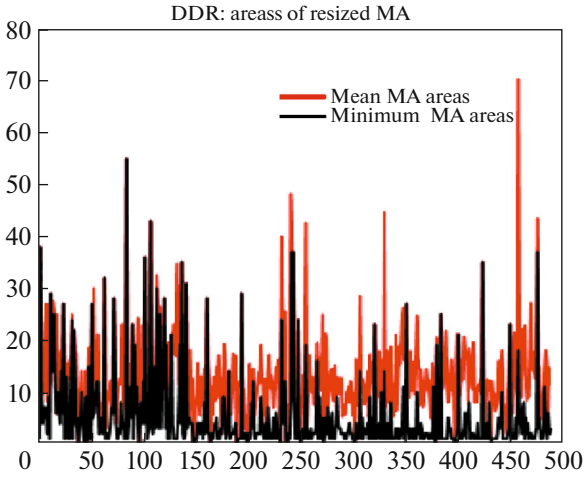

Fig. 9. Distribution of minimum (black curve) and mean areas of MAs in images from the DDR database in the cropped square of 512 × 512 pixels.

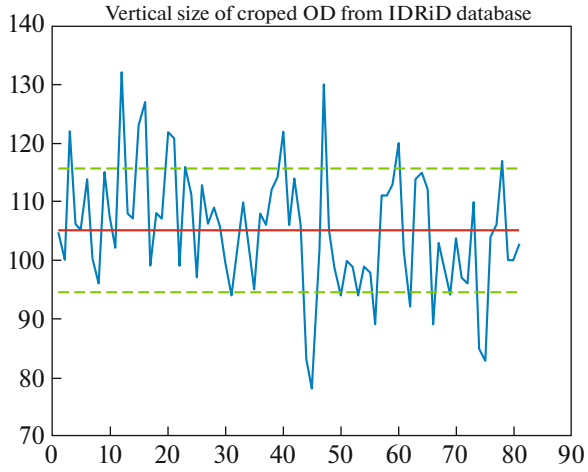

Fig. 10. Vertical sizes of ODs in the cropped square of 512 × 512 pixels.

preservation of information about the MAs available in the image.

CONCLUSIONS

We have studied the problem of choosing the optimal template for representing a digital retinal image of a human eye obtained by an arbitrary fundus-camera. In order to be objective, as experimental data, we used three databases created in different countries and containing MA masks generated by experienced ophthalmologists. The MA sizes may take on values in the range from 10 to 125 μm; i.e., they vary by more than an order of magnitude, and, in the digital representation, the differences may increase by one more orders of magnitude. For estimating the metric sizes of MAs in a digital image, we took the OD of a healthy human eye height as a reference value; the size of this height is similar in humans with normal eyes and is approximately 1880 μm. It is experimentally shown that, independently of the conditions of photographing of the retina, after cropping the square inscribed in the image and reducing the square to the size of 512 × 512 pixels, the image contains enough information for diagnosing the presence of DR in screening study. The template of the retinal image is universal and independent of the type of the fundus-camera used, the photography conditions, and the resolution of the obtained image. This template allows the development of a universal automated screening system of DR detection on the basis of machine-learning systems.

Table 5. Sizes of MAs and ODs in images of the IDRID base

Image no.	Number of MAs	min *h*	max *h*	min *w*	max *w*	*h* of OD	1 pixel in μm
01	18	12	34	12	33	548	3.43
01square	17	3	6	2	6	113	16.63
05	8	18	32	15	34	562	3.34
05square	6	4	7	3	7	119	15.80
09	54	15	48	14	54	618	3.04
09square	43	2	10	3	10	131	14.35
12	17	9	31	10	30	683	2.75
12square	15	1	6	1	6	129	14.57
15	7	11	23	12	28	613	3.06
15square	4	2	5	3	6	129	14.57
20	104	4	38	5	29	579	3.24
20square	77	1	10	1	8	122	15.41

FUNDING

The study was supported in part by the Belarusian Republican Foundation for Fundamental Research (project nos. F21PACG-001 and F22V-010). This paper was supported by the National Natural Science Foundation of China (project no. 61701049).

COMPLIANCE WITH ETHICAL STANDARDS

This article is a completely original work of its authors; it has not been published before and will not be sent to other publications until the *PRIA* Editorial Board decides not to accept it for publication.

Conflict of Interest

The process of writing and the content of the article do not give grounds for raising the issue of a conflict of interest.

REFERENCES

1. E. Decencière, G. Cazuguel, X. Zhang, G. Thibault, J.-C. Klein, F. Meyer, B. Marcotegui, G. Quellec, M. Lamard, R. Danno, D. Elie, P. Massin, Z. Viktor, A. Erginay, B. Laÿ, and A. Chabouis, "TeleOphta: Machine learning and image processing methods for teleophthalmology," IRBM **34**, 196–203 (2013). https://doi.org/10.1016/j.irbm.2013.01.010
2. DRIMDB (Diabetic Retinopathy Images Database) Database for Quality Testing of Retinal Images. https://academictorrents.com/details/99811ba62918f8e73791d21be29dcc372d660305. Cited January 5, 2022.
3. DRIVE: Digital Retinal Images for Vessel Extraction. https://drive.grand-challenge.org/. Cited January 5, 2022.
4. Y. Elloumi, M. Akil, and H. Boudegga, "Ocular diseases diagnosis in fundus images using a deep learning: approaches, tools and performance evaluation," Proc. SPIE **10996**, 109960T. https://doi.org/10.1117/12.2519098
5. E. Ezra, E. Keinan, Y. Mandel, M. E. Boulton, and Y. Nahmias, "Non-dimensional analysis of retinal microaneurysms: critical threshold for treatment," Integr. Biol. **5**, 474–480 (2013). https://doi.org/10.1039/c3ib20259c
6. S. S. Feman, "The natural history of the first clinically visible features of diabetic retinopathy," Trans. Am. Ophthalmol. Soc. **92**, 745–773 (1994).
7. Fundus Photography Overview. https://www.opsweb.org/page/fundusphotography. Cited January 5, 2022.
8. Kaggle-2015: Diabetic retinopathy detection. https://www.kaggle.com/c/diabetic-retinopathy-detection. Cited January 5, 2022.
9. G. Landa, R. B. Rosen, P. M. T. Garcia, and W. H. Seiple, "Combined three-dimensional spectral OCT/SLO topography and microperimetry: Steps toward achieving functional spectral OCT/SLO," Ophthalmic Res. **43** (2), 92–98 (2010). https://doi.org/10.1159/000247593
10. T. Li, Y. Gao, K. Wang, S. Guo, H. Liu, and H. Kong, "Diagnostic assessment of deep learning algorithms for diabetic retinopathy screening," Inf. Sci. **501**, 511–522 (2019). https://doi.org/10.1016/j.ins.2019.06.011
11. J. M. Molina-Casado, E. J. Carmona, and J. García-Feijoó, "Fast detection of the main anatomical structures in digital retinal images based on intra- and inter-structure relational knowledge," Comput. Methods Programs Biomed. **149**, 55–68 (2017). https://doi.org/10.1016/j.cmpb.2017.06.022
12. J. Moore, S. Bagley, G. Ireland, D. McLeod, and M. E. Boulton, "Three dimensional analysis of microaneurysms in the human diabetic retina," J. Anat. **194**, 89–100 (1999). https://doi.org/10.1046/j.1469-7580.1999.19410089.x
13. A. Noriega, D. Meizner, D. Camacho, J. Enciso, H. Quiroz-Mercado, V. Morales-Canton, A. Almaatouq, and A. Pentland, "Screening diabetic retinopathy using an automated retinal image analysis system in independent and assistive use cases in Mexico: Randomized controlled trial," JMIR Formative Res. **5**, e25290 (2021). https://doi.org/10.2196/25290
14. S. Nunes, I. Pires, A. Rosa, L. Duarte, R. Bernardes, and J. Cunha-Vaz, "Microaneurysm turnover is a biomarker for diabetic retinopathy progression to clinically significant macular edema: Findings for type 2 diabetics with nonproliferative retinopathy," Ophthalmologica **223**, 292–297 (2009). https://doi.org/10.1159/000213639
15. C. Pereira, D. Veiga, J. Mahdjoub, Z. Guessoum, L. Gonçalves, M. Ferreira, and J. Monteiro, "Using a multi-agent systemapproach for microaneurysm detection in fundus images," Artif. Intell. Med. **60**, 179–188 (2014). https://doi.org/10.1016/j.artmed.2013.12.005
16. P. Porwal, S. Pachade, R. Kamble, M. Kokare, G. Deshmukh, V. Sahasrabuddhe, and F. Meriaudeau, "Indian diabetic retinopathy image dataset (IDRiD): A database for diabetic retinopathy screening research," Data **3**, 25 (2018). https://doi.org/10.3390/data3030025
17. S. S. Puranik and V.B. Malode, "Morphology based approach for microaneurysm detection from retinal image," in *Int. Conf. on Automatic Control and Dynamic Optimization Techniques (ICACDOT), Pune, India, 2016* (IEEE, 2016), pp. 635–639. https://doi.org/10.1109/ICACDOT.2016.7877663
18. E. M. Shahin, T. E. Taha, W. Al-Nuaimy, S. El Rabaie, O. F. Zahran, and F. E. Abd El-Samie, "Automated detection of diabetic retinopathy in blurred digital fundus images," in *8th Int. Computer Engineering Conf. (ICENCO), Giza, Cairo, 2012* (IEEE, 2012), pp. 20–25. https://doi.org/10.1109/ICENCO.2012.6487084
19. A. K. Sjølie, R. Klein, M. Porta, T. Orchard, J. Fuller, H. H. Parving, R. Bilous, S. Aldington, and N. Chaturvedi, "Retinal microaneurysm count predicts progression and regression of diabetic retinopathy. Post-hoc results from the DIRECT Programme," Diabetic Med. **28**, 345–351 (2011). https://doi.org/10.1111/j.1464-5491.2010.03210.x

20. S. B. Sujith Kumar and V. Singh, "Automatic detection of diabetic retinopathy in non-dilated RGB retinal fundus images," Int. J. Comput. Appl. **47**, 26–32 (2012), pp. 26–32.

21. H. Wang, J. Chhablani, W. R. Freeman, C. K. Chan, I. Kozak, D.-U. Bartsch, and L. Cheng, "Characterization of diabetic microaneurysms by simultaneous fluorescein angiography and spectral-domain optical coherence tomography," Am. J. Ophthalmol. **153**, 861–867 (2012). https://doi.org/10.1016/j.ajo.2011.10.005

22. C. P. Wilkinson, F. L. Ferris III, R. E. Klein, P. P. Lee, C. D. Agardh, M. Davis, D. Dills, A. Kampik, R. Pararajasegaram, J. T. Verdaguer, and Global Diabetic Retinopathy Project Group, "Proposed international clinical diabetic retinopathy and diabetic macular edema disease severity scales," Ophthalmology **110**, 677–682 (2003). https://doi.org/10.1016/S0161-6420(03)00475-5

23. T. Y. Wong, J. Sun, R. Kawasaki, P. Ruamviboonsuk, N. Gupta, V. C. Lansingh, M. Maia, W. Mathenge, S. Moreker, M. M. K. Muqit, S. Resnikoff, J. Verdaguer, P. Zhao, F. Ferris, L. P. Aiello, and H. R. Taylor, "Guidelines on diabetic eye care: The international council of ophthalmology recommendations for screening, follow-up, referral, and treatment based on resource settings," Ophthalmology **125**, 1608–1622 (2018). https://doi.org/10.1016/j.ophtha.2018.04.007

24. L. Zhang, S. Feng, G. Duan, Y. Li, and G. Liu, "Detection of microaneurysms in fundus images based on an attention mechanism, Genes **10**, 817 (2019). https://doi.org/10.3390/genes10100817

Translated by E. Oborin

Valerii Vasil'evich Starovoitov, Doctor of Sciences and Professor of Computer Science. He is a principal research fellow at the United Institute of Informatics Problems, National Academy of Sciences of Belarus. Received the State Prize of the Republic of Belarus in Science. Research interests: processing and analysis of digital images obtained in different parts of the electromagnetic spectrum. He has published over 150 papers.

Yuliya Igorevna Golub, Candidate of Sciences, Associate Professor, Senior Research Fellow at the United Institute of Informatics Problems, National Academy of Sciences of Belarus.

Marina Mikhailovna Lukashevich, Candidate of Sciences, postdoctoral researcher at the Belarusian State University of Informatics and Radioelectronics. Research interests: digital image processing and machine learning.